 doi:10.20944/preprints202009.0014.v1

Article

New Mechanistic Insights on Carbon Nanotubes Nanotoxicity Using Isolated Submitochondrial Particles, Molecular Docking, and Nano-QSTR Approaches

Michael González-Durruthy [1,2,*], Riccardo Concu [1,*], Juan M. Ruso [2] and M. Natália D.S. Cordeiro [1]

[1] LAQV@REQUIMTE, Department of Chemistry and Biochemistry, Faculty of Sciences, University of Porto, 4169-007 Porto, Portugal.

[2] Soft Matter and Molecular Biophysics Group, Department of Applied Physics, University of Santiago de Compostela, 15782 Santiago de Compostela, Spain.

* Correspondence: michael.durruthy@fc.up.pt (M.G.-D.), Fax: +351220402659; ric.concu@gmail.com (R.C.), Fax: +351220402659.

Published:

Abstract: Herein, we present a combination of experimental and computational study on the mitochondrial F0F1-ATPase nanotoxicity inhibition induced by single-walled carbon nanotubes (SWCNT-pristine, SWCNT-COOH). To this end, the *in vitro* inhibition responses in submitochondrial particles (SMP) as F0F1-ATPase enzyme were strongly dependent on the concentration assay (from 3 to 5 μg/ml) for both types of carbon nanotubes. Besides, both SWCNTs show an interaction inhibition pattern like the oligomycin A (the specific mitochondria F0F1-ATPase inhibitor). Furthermore, the best crystallography binding pose obtained for the docking complexes based on the free energy of binding (FEB), fit well with the previous *in vitro* evidences from the thermodynamics point of view. Following an affinity order as: FEB (oligomycin A/F0-ATPase complex) = -9.8 kcal/mol > FEB (SWCNT-COOH/F0-ATPase complex) = - 6.8 kcal/mol ~ FEB (SWCNT-pristine complex) = -5.9 kcal/mol. With predominance of van der Waals hydrophobic nanointeractions with key F0-ATPase binding site residues (Phe 55 and Phe 64). By the other hand, results on elastic network models, and fractal-surface analysis suggest that SWCNTs induce significant perturbations by triggering abnormal allosteric responses and signals propagation in the inter-residue network which could affect the substrate recognition ligand geometrical specificity of the F0F1-ATPase enzyme in order (SWCNT-pristine > SWCNT-COOH). Besides, the performed Nano-QSTR models for both SWCNTs show that this method may be used for the prediction of the nanotoxicity induced by SWCNT. Overall, the obtained results may open new avenues toward to the better understanding and prediction of new nanotoxicity mechanisms, rational drug-design based nanotechnology, and potential biomedical application in precision nanomedicine.

Keywords: mitochondria; F0F1-ATPase; carbon nanotubes; computational nanotoxicology

Introduction

The coupled mechanical co-rotating between the γ and ε subunits that form the mitochondrial F1-ATP synthase (complex V) favors the H^+ protons flux necessary for ATP synthesis in all eukaryotic cells[1, 2]. This bioenergetic process involves several synchronized conformational changes which are critical for the survival or death of the cells[1-3]. In this regard, a few years ago has been shown that under pathological conditions like chronic

diseases as cancer, Alzheimer, Parkinson, MELAS syndrome, several toxic events, including nanotoxicity-induced by SWCNT may trigger F0F1ATPase dysfunction[3-5]. The ATP cellular reserves are abruptly consumed by a reverse biochemical reaction which paradoxically hydrolyses significant amounts of ATP compromising the cellular homeostasis and viability[3, 5].

Several chemical agents (including carbon nanoparticles) have shown a high affinity/selectivity by the bioenergetic mechanisms based on ATP hydrolysis[3, 5]. Particularly, nanoparticle-based single-walled carbon nanotubes (SWCNTs) which have been studied by its selective nanotoxicity effects on mitochondria (mitotropic behavior)[6-9].

To the best of our knowledge, the toxicological modulation of mitochondrial ATP bioenergetic mechanisms released by the exposure with SWCNT has been insufficiently characterized in order to explain the mitochondrial nanotoxicity-induced by SWCNT. By the other hand, this mechanistic knowledge could be very useful to implement strategies on the named "*precision mitochondrial nanomedicine*" to improve selectivity for the treatment of brain, cardiac diseases, and cancer using the mitotropic behavior of SWCNT to address active pharmacological principles as new targeting of the mitochondrial F0F1-ATPase[8-14]. In this context, we hypothesize that SWCNT could acts mimicking the pharmacodynamic behavior of the Oligomycin A, which is the specific inhibitor of the mitochondrial ATP-hydrolysis that modulate the activity of the c-ring-F0-ATP hydrolase subunit. The c-ring-F0-ATP hydrolase subunit represent an uncoupling channel which is part of the mitochondrial permeability transition pore-induced associated to mitochondrial dysfunction and apoptosis[15, 16]. Following this idea, we suggest that SWCNT could promote the selective inhibition of the F0-ATPase under pathological conditions[16-20].

In this regard, computational approaches like molecular docking simulation, elastic network models, fractal-surface approaches linked to nano-quantitative-structure-toxicity relationships (Nano-QSAR/QSTR models) and others[8, 21-24], could be efficiently applied to the exhaustive exploration of the underlying mechanisms of mitochondrial bioenergetic dysfunction (pathological ATP-hydrolysis) from the structural point of view for therapeutic purposes.

Particularly, computational Nano-QSAR/QSTR approaches are essential tools to support the discovery process of toxicological effects of nanomaterials (SWCNT). Several approaches have been developed and applied recently able to predict potential harmfulness of nanoparticles and nanomaterials[8-14]. One of the most used is the so called nano-quantitative-structure-toxicity-relationships (Nano-QSTR models) due to the fact that was successfully applied in very different fields[25-27]. This in silico tools have the quality of being versatile and reconfigurable to many problems. For example, the nano-quantitative-structure-binding-relationship (Nano-QSBR) models is a type of Nano-QSTR which is able to associate the physico-chemical properties of nanomaterials (nanodescriptors) with the theoretical free energy of binding (FEB values, kcal/mol) obtained from the molecular docking studies and also to experimental nanotoxicological outputs[13, 14, 28].

Due to this, QSAR (Nano-QSTR) paradigm has been applied since the beginning of the "nano revolution" as a useful methodology able to support toxicity profiling of nanomaterials and CNT [29-33]. Several approaches by many authors have been reported combining different molecular descriptors, methodologies and algorithms, including machine learning and deep learning[32-40]. In this sense, in strongly advisable use Nano-QSTR approaches while performing toxicity profiling of CNT and nanomaterials also considering *in silico* approaches are strongly encouraged by authorities in order to improve the EU 3R principles (replacement, reduction, refinement) in Alternative Toxicology. Currently, the main limitation of these computational methods is to address a feasible mechanistic interpretation of the nanotoxicity phenomena at the atomic level, in many cases[41].

Then, in this work we propose for the first time, a combination of computational modeling approaches, based on molecular docking simulations, elastic network models, fractal-surface approaches and Nano-QSTR calculations, along with experimental validation to tackle the study of binding interactions between single-walled carbon nanotubes with the mitochondrial F0F1-ATPase

Preprints (www.preprints.org) | NOT PEER-REVIEWED | Posted: 1 September 2020 doi:10.20944/preprints202009.0014.v1

toward to contribute to the rational drug-design based nanotechnology, mitotarget-drug discovery and the new area of precision mitochondrial nanomedicine.

Materials and methods

Isolation of rat-liver sub-mitochondrial particles (SMP).

The frozen RLM pellet was thawed and diluted with homogenization medium to contain 20 mg of protein/ml. The mitochondrial suspension was subjected to sonic oscillation four times for 15 s with 30 s intervals, using 80 watts at 4°C[42-45]. The suspension was then centrifuged at 9750 x g for 10 min at 4°C and the submitochondrial particles in the supernatant were isolated by additional centrifugation in a Sorval SV-80 vertical rotor for one hour at 15 000 rev/min at 4°C, using discontinuous gradient containing 1ml of 0.5 M sucrose and 1 ml of 2.0 M sucrose in 5 mM Tris-HCl, pH 7.4. Finally, the SMP were suspended in the isolation medium, and the final volume adjusted to give a stock suspension containing 1 mg of protein/ml.

Standard incubation procedure.

Mitochondria liver isolated and submitochondrial particles (SMP) were energized with 5 mM of potassium succinate (plus 2.5 μM of rotenone) in a standard incubation medium consisting of 125 mM of sucrose, 65 of mM KCl, 2 mM of inorganic phosphate (K_2HPO_4) and 10 mM of HEPES-KOH pH 7.4 at 30 °C.[42-45]

Determination of mitochondrial F0F1-ATPase inhibition in isolated rat-liver sub-mitochondrial particles (SMP).

Isolated rat-liver sub-mitochondrial particles (isolated-F0F1-ATPase) (20 mg of protein) were incubated according the following experimental groups: **1)** untreated SMP, **2)** SMP + DMSO (100 mM), **3)** SMP+ SWCNT-samples (SWCNT-pristine, SWCNT-COOH) in the range of concentration of (0.5-5 μg/ml), **4)** SMP + Oligomycin A (1 μM) as positive control, and **5)** SMP + Oligomycin A (1 μM) + SWCNT-samples at 5 μg/ml as additional control assay. The reactions are started by addition of enzyme as H^+-c-ring/F_0-ATPase (80 μg of protein). The total volume was 1ml. After 10 min at 37°C, the reaction was stopped by addition of 0.5 trichloroacetic acid, 30% (w/v). Phosphate released by ATP hydrolysis is measured on 0.5 ml of molybdate reagent (10 mM ammonium molybdate in 2.5 M sulfuric acid), 1 ml of acetone and 0.5 ml of 0.4 M citric acid. After each addition, the tubes are homogenized for 10 s in a vortex mixer. The mitochondrial F0F1-ATPase inhibition (F0-ATPase inhibition) for each treatment was calculated by measuring the absorbance at 355 nm[42-45]. Before all spectrophotometric F0-ATPase inhibition measurements, the blanks with each SWCNT were run and interferences absorbance peaks of SWCNT were not observed at 300–400 nm[42-45]. Furthermore, each SWCNT-sample was added under continuous stirring by using magnetic stirrer cuvettes.

Statistical procedures for the mitochondrial assays using SMP.

Analysis of variance (ANOVA) followed by a post hoc Newman–Keuls multiple comparison test to determine statistical differences between F_0-ATPase inhibition assay experimental groups was performed. All the biochemical tests by using isolated rat-liver mitochondria (RLM) and sub-mitochondrial particles (SMP) were performed at least three times in triplicate. Normality and variance homogeneity were verified using Shapiro–Wilks and Levene tests, respectively, before using ANOVA analysis. In all cases, significance level was set in 5%.

Molecular docking study

Docking simulations were performed using Autodock tools mixed Autodock Vina to understand the strength of biochemical interactions across CNT-family member (pristine-CNT, CNT-OH, CNT-COOH), and oligomycin A on F0-ATPase. These binding *in silico* interactions were

Preprints (www.preprints.org) | NOT PEER-REVIEWED | Posted: 1 September 2020 doi:10.20944/preprints202009.0014.v1

performed only to explain hidden biophysical and pharmacodynamic mechanisms observed in the mitochondrial *in vitro* assays. For this instance, it was modeled only three types of single walled zig-zag SWCNTs (Hamada index n = 8, m = 0) like SWCNT(8.0), SWCNT-COOH(8.0) and SWCNT-OH(8.0) as F0F1-ATPase ligands in order to reproduce and modeling some critical experimental conditions from CNT-properties like CNT-functionalization linked to observed F0-ATPase inhibition (ATP-hydrolysis inhibition) in isolated-RLM and isolated-SMP. Following this idea, the F0F1-ATPase C10 ring with oligomycin A from yeast (*Saccharomyces cerevisiae*) as the receptor (PDB ID: 5BPS, Resolution 2.1Å) was obtained from the *RCSB Protein Data Bank* (PDB)[46]. It is important to note that, c-ring-F0-ATPase subunit.pdb x-ray structure from *Saccharomyces cerevisiae* (5BPS) can be used in the context of the present docking approaches taking into account that mitochondrial c-ring-F0-ATPase subunit.pdb x-ray structure from *Rattus norvegicus* with oligomycin A has not been crystallized and included in the *RCSB Protein Data Bank*[46]. However, the oligomycin A-pharmacodynamics mechanism is highly conserved in *Rattus norvegicus* according to previous experimental evidences[17].

Before the molecular docking, ATPase C10 ring molecular structure was optimized using the AutoDock Tools 4 software for AutoDock Vina. The algorithm includes the removal of crystallographic water molecules and all the co-crystallized ATPase C10 ring ligand molecules, such as Oligomycin A (Oligo A: $C_{45}H_{74}O_{11}$ like ID: EFO) from ATPase C10 ring chains (B, E, K, L, M, O). Oligomycin A a recognized classical inhibitor of F0F1-ATPase inhibition it was used as a control to compare the affinity and/or relevant interactions by re-docking procedure.

This theoretical algorithm was performed to the c-ring F0-ATPase subunit using a grid box size with dimensions of X= 22 Å, Y= 22 Å, Z= 22 Å and the c-ring F0-ATPase subunit grid box center X=19.917 Å, Y= 19.654 Å, Z= 29.844 Å to evaluate the SWCNT-c-ring F0-ATPase interaction[47], considering the oligomycin A environment to evaluate the SWCNT-surface affinity in the c-ring F0-ATPase subunit active binding site.

The docking free energy of binding output results (or FEB values) is defined by affinity (like ΔG_{bind} values) for all docked poses of the formed complexes (SWCNT-F0ATPase) and include the internal steric forces of a given ligands (SWCNT) which can be expressed as the sum of individual molecular mechanics terms of standard-chemical potentials as: van der Waals interactions (ΔG_{vdW}), hydrogen bond ($\Delta G_{H\text{-}bond}$), electrostatic interactions ($\Delta G_{electrost}$), and intramolecular interactions ($\Delta G_{internal}$) ligands (SWCNTs) from empirically validated Autodock Vina scoring function based on default Amber force-field parameters[21-23].

Then the (SWCNTs-F0-ATPase) complexes free energy of binding (FEB_{dock}) was calculated based on the following scoring function:

$$FEB_{dock} \approx \Delta G_{bind} = \Delta G_{vdW} + \Delta G_{H-bond} + \Delta G_{electrost} + \Delta G_{\text{int}} \quad (1)$$

$$FEB_{dock} \approx \Delta G_{bind} = \Delta G_{vdW} \sum_{SWCNT-F0ATPase} \left(\frac{A_{ij}}{d_{ij}^{12}} - \frac{B_{ij}}{d_{ij}^{6}} \right) + \Delta G_{H-bond} \sum_{SWCNT-F0ATPase} E(t) \left(\frac{C_{ij}}{d_{ij}^{12}} - \frac{D_{ij}}{d_{ij}^{10}} \right) + \Delta G_{elec} \sum_{SWCNT-F0ATPase} 332.0 \frac{q_i q_j}{\epsilon(d_{ij}) d_{ij}} +$$

$$\Delta G_{internal} \left\{ \sum_{SWCNT} \frac{A_{ij}}{d_{ij}^{12}} - \frac{B_{ij}}{d_{ij}^{6}} + \sum_{SWCNT} E(t) \times \left(\frac{C_{ij}}{d_{ij}^{12}} - \frac{D_{ij}}{d_{ij}^{10}} \right) + \sum_{SWCNT} 332.0 \frac{q_i q_j}{4 d_{ij} d_{ij}} + \sum_{SWCNT} \gamma_k \left(1 + \cos\left(\varpi_k \theta_k - \theta_{0k}\right)\right) \right.$$

(2)

$\Delta G = -RT(\ln K_i)$, R (gas constant) is 1.98 cal*(mol*K)$^{-1}$, and K_i represents the predicted inhibition constants at T = 298.15 K. The first term describes the *van der Waals* interaction as A_{ij}/d_{ij}^{12} (attractive Guassian function) and B_{ij}/d_{ij}^{6} (repulsive hyparabolic function) to represent a typical

Preprints (www.preprints.org) | NOT PEER-REVIEWED | Posted: 1 September 2020 doi:10.20944/preprints202009.0014.v1

Lennard-Jones potential (SWCNT-F0ATPase). The Gaussian term is negative and the parabolic positive, d_{ij} is the surface distance calculated as $d_{ij} = r_{ij} - R_i - R_j$, where r_{ij} is the interatomic distance and R_i and R_j are the radii of the atoms in the pair of interaction of $SWCNT_i$-$F0ATPase_j$ atoms. The second term is the pair consisting of an H-bond donor and an H-bond acceptor as a directional 12-10 hydrogen-bonding potential term such as C_{ij}/d_{ij}^{12} and D_{ij}/d_{ij}^{10} (H-bonding potential with Goodford directionality), where $E(t)$ is an angular weight factor to represents the hydrogen bonds directionality and d_{ij} follows the criteria mentioned above. Atoms with d_{ij} below of cutoff value of 7 Å were considered as interacting atoms[21-23].

The third term represents the Coulomb electrostatic potential stored for the formed complex $(SWCNT/F0ATPase)_{ij}$ of N charges (q_i, q_j) of pairs of charged atoms of $SWCNT_{(i)}$ and $F0ATPase_{(j)}$. For this instance, appropriated Gasteiger partial atomic charges of the F0ATPase enzyme were assigned. Herein, d_{ij} is the interatomic distance between the point charges as the reference positions of interaction based on distance-dependent dielectric constant. Herein, Autodock Vina based on Amber force field was parameterized with default options for the pristine-SWCNT, SWCNT-OH and SWCNT-COOH by summing up individual molecular mechanic contributions like: SWCNT-intra-molecular contributions, SWCNT-aromaticity criterion and the set number of active torsions moving of each SWCNT-ligand following to general preparation procedures of ligand. For this instance, the fourth term of the **equation (2)** as ($\Delta G_{internal}$) was used to validate the internal steric energy of each SWCNT-ligand including dispersion-repulsion energy and a torsional energy through the sum of the default Amber force field parameters (ligand conformation-independent parameters of the Autodock Vina scoring function)[21-23].

It is important to note that, docking dimensionality based on degree of freedom (DOF) for each SWCNT (SWCNT-pristine, SWCNT-COOH) like: SWCNT-atom position/translation (x_i, y_i, z_i = 3), SWCNT-atom orientation/quarternion ($q(x_i)$, $q(y_i)$, $q(z_i)$, $q(w_i)$ = 4), SWCNT-number of rotable bonds/torsion (tor_1, tor_2, …, $tor_n = N_{tor}$) and SWCNT-total dimensionality (total DOF = 3 + 4 + n) not have a significant weight in the FEB_{dock} based on the very small intra-molecular contributions of force field parameters of the SWCNT-ligand which were considered as rigid-bodies and considering the SWCNT-geometry optimization by $\Delta G_{internal}$ minimization of the SWCNT-ligands used in the present study [21-23].

Local-perturbation response induced by SWCNT on the F0-ATPase subunit.

In parallel with docking simulation a new model based elastic network model was performed to propose potential mechanism-based on the SWCNT-propensity to perturb the intrinsic motion of F0-ATPase subunit binding residues involved in the docking interactions. To this purpose, the F0-ATPase is represented as a network, or graph of the inter-residue contacts from Cα-F0-ATPase atoms of a residue and the overall potential is simply the sum of harmonic potentials between interacting nodes (F0-ATPase residues). The network includes all interactions within a cutoff distance < 4 Å. Information about the orientation of each interaction with respect to the global coordinates system is considered within the force constant matrix and allows prediction of perturbed anisotropic motions[48]. The force constant of the F0-ATPase protein system can be described by a Kirchhoff or Hessian matrix ($H_{i,j}$) to evaluate potential perturbations induced by SWCNT-ligand in the transduction properties of the F0-ATPase enzyme according to the following equation:

$$H_{i,j} = \begin{bmatrix} H_{1,1} & H_{1,2} & \cdots & H_{1,N} \\ H_{2,1} & H_{2,2} & \cdots & H_{2,N} \\ . & . & \cdots & . \\ H_{N,1} & H_{N,2} & \cdots & H_{N,N} \end{bmatrix} \quad (3)$$

Preprints (www.preprints.org) | NOT PEER-REVIEWED | Posted: 1 September 2020 doi:10.20944/preprints202009.0014.v1

Where each $H_{i,j}$ is a 3×3 matrix which holds the anisotropic informations regarding the orientation of residues (i, j-nodes). Each such sub matrix (or the "super element" of the $H_{i,j}$ –Hessian matrix) is defined by the equation 4 as:

$$H_{i,j} = \begin{bmatrix} \partial^2 V/\partial X_i \partial X_j & \partial^2 V/\partial X_i \partial Y_j & \partial^2 V/\partial X_i \partial Z_j \\ \partial^2 V/\partial Y_i X_j & \partial^2 V/\partial Y_i \partial Y_j & \partial^2 V/\partial Y_i \partial Z_j \\ \partial^2 V/\partial Z_i X_j & \partial^2 V/\partial Z_i \partial Y_j & \partial^2 V/\partial Z_i \partial Z_j \end{bmatrix} \quad (4)$$

The second partial derivatives are the harmonic potentials V between interacting F0-ATPase residues. These partial derivatives are formed by a simple matrix of cosines and the off-diagonal super elements of the $H_{i,j}$ –Hessian matrix are calculated according to equation 5 as:

$$H_{i,j} = \begin{bmatrix} -\gamma \frac{(X_j - X_i)(X_j - X_i)}{s_{i,j}^2} & -\gamma \frac{(X_j - X_i)(Y_j - Y_i)}{s_{i,j}^2} & -\gamma \frac{(X_j - X_i)(Z_j - Z_i)}{s_{i,j}^2} \\ -\gamma \frac{(Y_j - Y_i)(X_j - X_i)}{s_{i,j}^2} & -\gamma \frac{(Y_j - Y_i)(Y_j - Y_i)}{s_{i,j}^2} & -\gamma \frac{(Y_j - Y_i)(Z_j - Z_i)}{s_{i,j}^2} \\ -\gamma \frac{(Z_j - Z_i)(X_j - X_i)}{s_{i,j}^2} & -\gamma \frac{(Z_j - Z_i)(Y_j - Y_i)}{s_{i,j}^2} & -\gamma \frac{(Z_j - Z_i)(Z_j - Z_i)}{s_{i,j}^2} \end{bmatrix}$$

(5)

where γ is an interaction constant. The $s_{i,j}$ is the instantaneous distance between nodes or residues *i* and *j*. The diagonal super elements are calculated by:

$$H_{i,i} = -\sum_{j=1, j\neq i}^{N} H_{i,j} \quad (6)$$

Herein, the force constant matrix $H_{i,j}$ holds information regarding the F0-ATPase-residues position/orientation. The inverse of the *Hessian* matrix is the covariance matrix of *3N* multi-variant Gaussian distribution where *p* is an empirical parameter according to the equation (7) for the new off-diagonal elements of the *Hessian* matrix which hold the desired information on the residue-fluctuations including the F0-ATPase binding-site residues (i, j) involved in the SWCNT-F0-ATPase docking interactions.

$$H_{i,j} = -\frac{1}{s_{i,j}^{p+2}} \begin{bmatrix} (X_j - X_i)(X_j - X_i) & (X_j - X_i)(Y_j - Y_i) & (X_j - X_i)(Z_j - Z_i) \\ (Y_j - Y_i)(X_j - X_i) & (Y_j - Y_i)(Y_j - Y_i) & (Y_j - Y_i)(Z_j - Z_i) \\ (Z_j - Z_i)(X_j - X_i) & (Z_j - Z_i)(Y_j - Y_i) & (Z_j - Z_i)(Z_j - Z_i) \end{bmatrix}$$

(7)

Then, we tackle the construction of the local perturbation response scanning maps (LPRS maps) by setting the following conditions: i) unbound F0-ATPase as the control simulation experiment, ii) oligomycin A + F0-ATPase, iii) SWCNT-pristine + F0-ATPase, and SWCNT-COOH + F0-ATPase.

Performing Nano-QSTR approaches

The Nano-QSTR models have been developed using a linear regression approach to predict the mitochondrial F0F1-ATPase inhibition values of the SWCNT herein studied. The values used for the development of the continuous model were obtained from molecular docking experiments considering the free energy of binding (FEB values) obtained from the complexes SWCNT-pristine/F0-ATPase, and SWCNT-COOH/F0-ATPase. For this purpose, two different sets for both

Preprints (www.preprints.org) | NOT PEER-REVIEWED | Posted: 1 September 2020 doi:10.20944/preprints202009.0014.v1

ligands (SWCNT-pristine, SWCNT-COOH) were efficiently built. Considering the three recognized categories of geometric topologies as: zig-zag-SWCNT (Hamada index m = 0, n > 0), amchair-SWCNT (Hamada index m = n) and chiral-SWCNT, characterized by Hamada index (n, m), with m > 0 and m ≠ n; and with its enantiomers (or mirror images) present Hamada index (m,n), which is different from (n, m) no reflection symmetry[13, 14]. Then, regression Nano-QSTR models were developed using the linear regression tool implemented in the Statistica® suite.

The validation of the Nano-QSTR model was performed using the cross-validation module implemented in the software. This procedure is aimed at assessing the predictive accuracy of a model. The test randomly split the dataset into a training set and a validation set, ensuring that if an entry was included in the test set it could not be used in the validation test. In so doing, the model was developed using the cases in the training or learning sample, which, in our study, was 70% of the dataset. The predictive accuracy was then assessed using the remaining 30% of the dataset.

Finally, the performance of the model was evaluated using the residuals, *R* and R^2 and other relevant statistics. Regarding the molecular descriptors (MD), we used the DRAGON 7.0® software to calculate the variables that have been used for the development of the models. This software suite is able to calculate up to 7,500 different descriptors, belonging to very different classes, such as topological, 2D, 3D, connectivity, and so on[49]. In order to select the best subset of MD, we have performed a feature selection process using a forward stepwise methodology[33] for both models. At the end of this procedure, we were able to develop the pristine and the carboxylate model using respectively two and three MD belonging to the Topological class. The two MD used in the SWCNT-pristine model are the Narumi geometric topological index (GNar) and the electro-topological positive variation (MAXDP). The Narumi index of a graph *G* is defined as the product of degrees of all its vertices:

$$\mathrm{NK}(G) = \prod_{i=1}^{n} d_G(v_i) \qquad (8)$$

The MAXDP is calculated as follow:

$$S_i = I_i + \Delta I_{i=} I_i + \sum_{J0i}^{nSK} \frac{I_i - I_j}{(a_{ij}+1)^k} \qquad (9)$$

which is calculated as the maximum positive value of ΔIi.

Regarding the SWCNT-COOH model, the continuous model was developed using three MD, one is the same GNAR used for the pristine model. The other two are defined as follow. The first one is the path/walk Randic shape indices that is calculated by summing, over the non-H atoms, the ratios of the atomic path count over the atomic walk count of the same order k and, then, dividing by the total number of non-H atoms (nSK). Since path/walk count ratio is independent of molecular size, these descriptors can be considered as measures of molecular shape. Dragon calculates path/walk shape indices from order 2 up to 5; the index of first order is not provided as the counts of the paths and walks of length one is equal and, therefore, the corresponding molecular index equals one for all molecules. The formula in this case is not reported in the Dragon manual.

Finally, the last molecular descriptor used is the so called lopping centric index (LOC), which is calculated as the mean information content derived from the pruning partition of a graph:

$$LOC = \sum k \frac{n_k}{nSK} * log_2 \frac{n_k}{nSK} \qquad (10)$$

where nk is the number of terminal vertices removed at the *k*th step and nSK the number of non-H atoms.

Results and Discussion

CNT effects on sub-mitochondrial particles (SMP).

Preprints (www.preprints.org) | NOT PEER-REVIEWED | Posted: 1 September 2020 doi:10.20944/preprints202009.0014.v1

Herein, we present the *in vitro* assay on the inhibitory effect of the SWCNT-ligands (SWCNT-pristine, SWCNT-COOH) at the range of concentration of 0.5-5 μg/ml over F0-ATPase using isolated rat-liver sub-mitochondrial particles (isolated F0F1-ATPase) from mitochondrial inner membrane. In general, we can see that the SWCNT-tested exhibit high ability to act as F0-ATPase inhibitors (ATP-hydrolysis) at a range of concentration of 3-5 μg/ml. Besides, a concentration dependence with significant statistical difference ($p < 0.05$) when compared with SMP (untreated-SMP group) and the DMSO-treated SMP was observed. We note an oligomycin A-like pattern (positive control group used) for both SWCNT-ligand in a range of concentration of 3-5 μg/ml without significant statistical difference ($p > 0.05$) when compared with oligomycin A (**Figure 1**). According to this, the treated-SMP from mixed CNT-ligand (5μg/ml) plus oligomycin A (1μM) showed strongest F0-ATPase inhibition ($p < 0.05$) when compared with untreated-SMP and the DMSO-treated SMP, and the remaining CNT-treated-SMP (3-5 μg/ml). Suggesting a strong synergistic effect on F0-ATPase inhibition (mitochondrial nanotoxicity). Details of these experimental results can see in Figure 1.

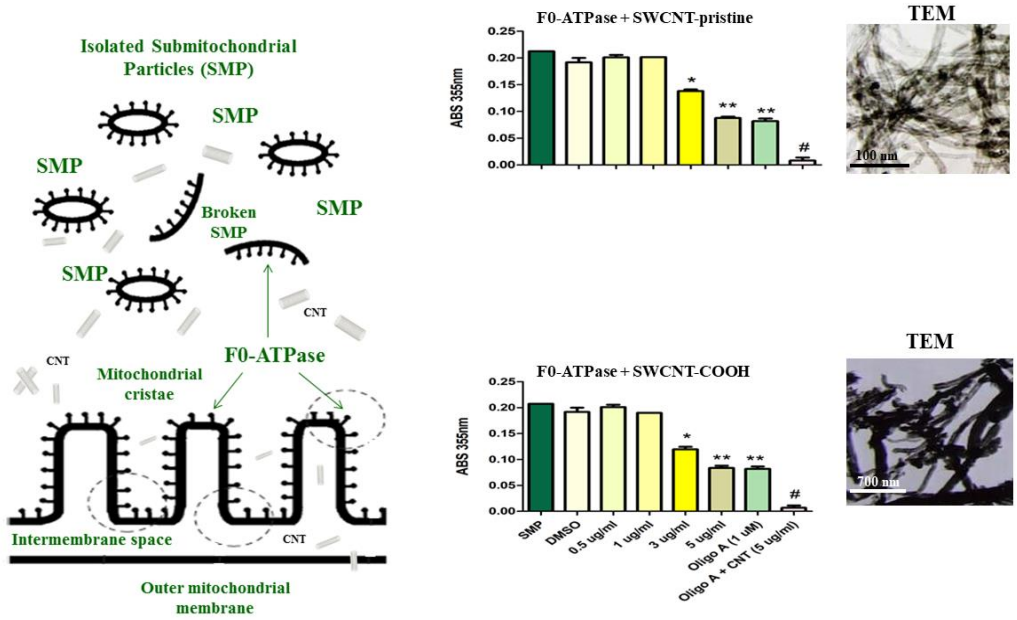

Figure 1. Representative results of F0-ATPase inhibition behavior-induced by SWCNT-pristine, SWCNT-COOH on isolated-rat liver submitochondrial particles (SMP). Experimental conditions are described under **Methods** section. Different treatments are depicted like untreated-submitochondrial particles control (SMP), DMSO-treated SMP, CNT-treated SMP (1-5μg/ml), Oligomycin A-treated SMP (F0F1-ATPase inhibitor used as positive control) and treated-SMP with mixed SWCNT-ligand (5μg/ml) + Oligomycin A(1μM) to mimicking synergistic effects on F0-ATPase inhibition was performed as additional control group. Results are representative of three experiments (n=3). Symbols (*, **, #) were used to denote statistical differences ($p < 0.05$). On the far right we show the TEM image obtained for the samples of SWCNT-pristine, SWCNT-COOH.

Modeling F0ATPase inhibition induced by SWCNTs

Herein, molecular docking was carried out in order to evaluate the influence of the carbon nanotubes (SWCNT-pristine and SWCNT-COOH) in the F0-ATPase inhibition response. Herein, the best docking binding pose from each modeled-CNT (SWCNT-pristine, SWCNT-COOH), theoretically suggest that these CNT could act in the same biophysical environment that the oligomycin A based on hydrophobic non-covalently interaction (π-π interactions) involving phenylalanine hydrophobic residues (Phe 55 and Phe 64 of the chains C, D and M), which are critically involved in the F0-ATPase inhibition (ATP-hydrolysis) in the F0-ATPase subunit active binding-site. See Figure 2.

Preprints (www.preprints.org) | NOT PEER-REVIEWED | Posted: 1 September 2020 doi:10.20944/preprints202009.0014.v1

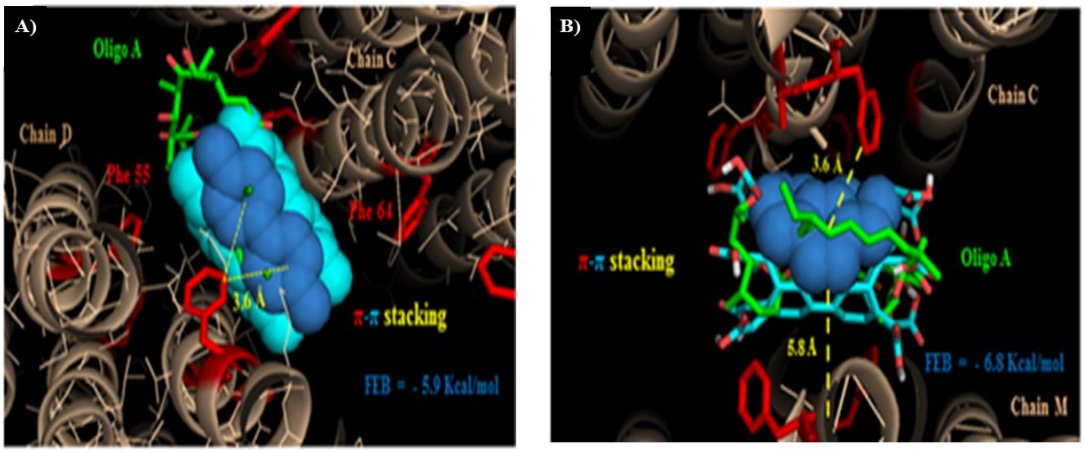

Figure 2. Snapshots selection from molecular docking interactions obtained from the best binding poses of the ligands as **A**) superimposed representation of oligomycin A and SWCNT-pristine, and **B)** superimposed representation of oligomycin and SWCNT-pristine SWCNT-COOH interacting with critical phenylalanine hydrophobic residues (Phe 55 and Phe 64: labelled red) which belong to the target chains C, D and M in F0-ATPase subunit receptor. Please, note that Oligomycin A (labelled green) corresponds to the control simulation experiment used here as reference due to this ligand is the specific inhibitor of the F0-ATPase in all cases.

The free energy of binding (FEB)-values of the formed docking complexes following the order: FEB (oligomycin A/F0-ATPase complex) = -9.8 kcal/mol > FEB (SWCNT-COOH/F0-ATPase complex) = -6.8 kcal/mol ~ FEB (SWCNT-pristine complex) = -5.9 kcal/mol with interatomic distance of interaction lower than 5 Å, in all the cases. Besides, we note that the presence of π-π interactions like Y-shaped and pseudo parallel-displaced motif-orientation preferences for both single-walled carbon nanotubes. Besides, a more electrostatically favored interactions in the CNT-sidewall than the CNT-tips were observed in both simulations (SWCNT-pristine and SWCNT-COOH). Probably, due to better orientation and stability between the planar-benzene-quadrupoles formed between van der Waals surface from the modeled-SWCNT and the phenylalanine hydrophobic residues (Phe 55 and Phe 64) of the F0-ATPase binding site and interacting in the same biophysical environment that the F0-ATPase specific inhibitor (oligomycin A)[17].

Next, we carried out the theoretical modeling based on the local perturbation response scanning maps (LPRS-maps). The LPRS maps are based in elastic network models (ENM models) and have been widely recognized to study relevant conformational changes of target proteins (as F0-ATPase under unbound and bound states) at the atomistic and molecular level[48], It is well-known that the ENM models could explain a large number the conformational differences based on the perturbation pattens of the network formed by the target residues evaluated (Phe 55 and Phe 64) For this instance, LPRS maps generates a comprehensive visualizations of the F0-ATPase inhibition response which allows evaluate allosteric signal propagations in response to external perturbations under the presence of a given ligand (i.e., the oligomycin A as F0-ATPase-specific inhibitor, SWCNT-pristine, and SWCNT-COOH. The results can see in the **Figure 3.**

Preprints (www.preprints.org) | NOT PEER-REVIEWED | Posted: 1 September 2020 doi:10.20944/preprints202009.0014.v1

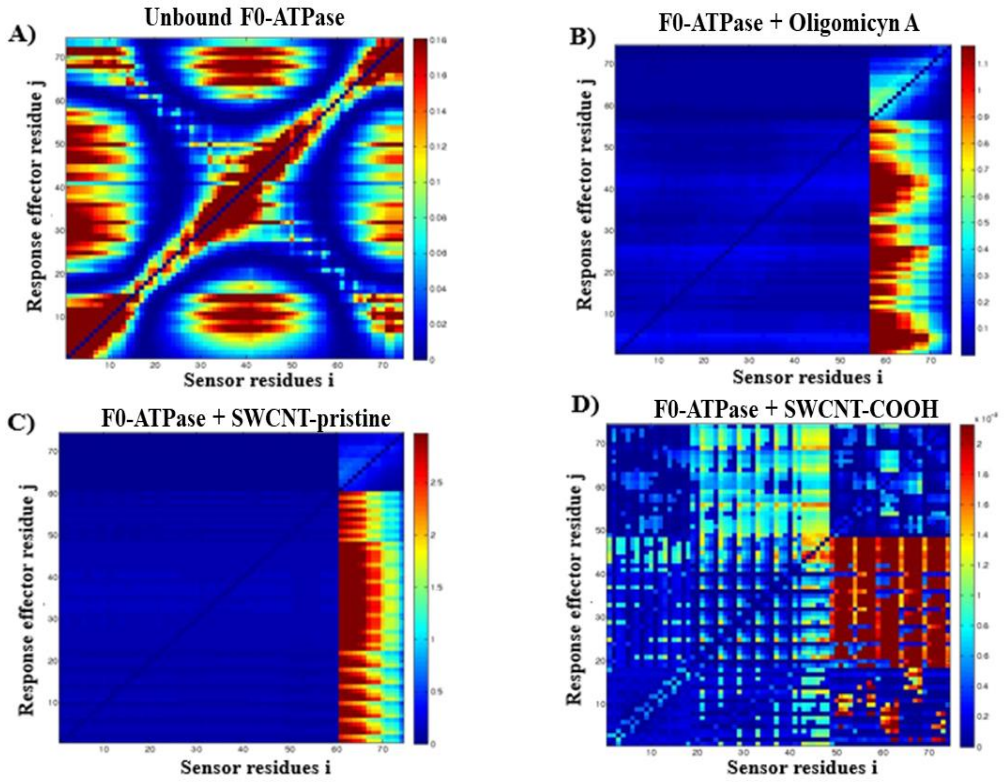

Figure 3. Perturbation response analysis for the F0-ATPase inhibition response. **A)** LPRS map obtained for the unbound F0-ATPase as the control simulation experiment. Individual LPRS-maps obtained from the best docking complexes (in the bound state for all the ligands tested) with intensity bar color (on the right) for: **B)** oligomycin A/F0-ATPase complex, **C)** SWCNT-pristine/F0-ATPase complex, and **D)** SWCNT-COOH/ F0-ATPase complex. All the LPRS-maps were established in range of the low frequency normal modes in order to capture relevant fluctuations associated with F0-ATPase catalytic function.

The results on LPRS-maps show that both single-walled carbon nanotubes promote a significant change in the perturbation patterns of the network of target residues compared with the physiological condition represented by the unbound state of F0-ATPase. In this regard, we note abrupt perturbations in several blocks of residues more pronounced for the SWCNT-pristine (strong F0-ATPase inhibition) than the SWCNT-COOH (moderate F0-ATPase inhibition) during the interaction with the F0-ATPase. Interestingly, the LPRS map of the SWCNT-pristine/F0-ATPase complex mimicking the toxicodynamic behavior of the oligomycin A/F0-ATPase complex inducing strong F0-ATPase inhibition (See Figure **Figure 3, B and C**) suggesting a similar pattern of allosteric network perturbation. However, the LPRS map obtained from the SWCNT-COOH/F0-ATPase complex exhibits a pattern of perturbation closer to the physiological condition maintaining a certain coupling between the residues composing the F0-ATPase network suggesting the presence of a moderate nanotoxicity-based F0-ATPase inhibition. The relevance of these results is that strong local perturbations promote triggering strong allosteric responses in the j-effector residues from F0-ATPase receptor affecting its mitochondrial catalytic function involving the signal transduction of the perturbations from the block of i-sensor residues which trigger abnormal signals propagation across inter-residue network for j-effector F0-ATPase residues. We could suggest that considering the SWCNT-docking position, both ligands (SWCNT-pristine >> SWCNT-COOH) can theoretically disrupt the H^+-proton flux dynamic in the mitochondrial H^+-F0-ATPase subunit, compromising the coupling between oxidative phosphorylation and electron transport in the respiratory chain inducing potential bioenergetic dysfunction and the mitochondria nanotoxicity[8].

In order to quantify potential fractal geometrical perturbations, a fractal surface analysis was carried out to model changes-based perturbations in the geometric surface of the binding effector

Preprints (www.preprints.org) | NOT PEER-REVIEWED | Posted: 1 September 2020 doi:10.20944/preprints202009.0014.v1

residues of the F0-ATPase under unbound and bound state (*i.e.*, under SWCNT-pristine and SWCNT-COOH interactions)[8]. To this end, several fractal dimensions (FDs namely: D_{BW}, D_{BBW} and D_{WBW}) were calculated using the box-counting methods from the LPRS maps previously obtained[50]. The Fractal Theory allows the mathematical modeling of the geometric complexity (across multiple scales) and self-similarity (scale-invariant structure) from non-Euclidean real or virtual objects (as SWCNT-tested). One of the most important properties in the fractal modeling is the degree of self-similarity. Then, a topological fractal dimension near to 2 is categorized-like high complexity (high variety of geometrical information) and low self-similarity, in opposite a topological fractal dimension closer to 1 informs about little complexity and high self-similarity. Herein, the non-Euclidean geometrical patterns were included according to the fractal dimension like FD_{BW}, that describes the surface geometric perturbations in the border of LPRS map fractal pattern[50]. The FD_{B+BW}, characterizes the surface geometric perturbations on the white background, and the FD_{W+BW} the fractal perturbations pattern on the black background from the LPRS images calculated for each simulation conditions. See **Figure 4**.

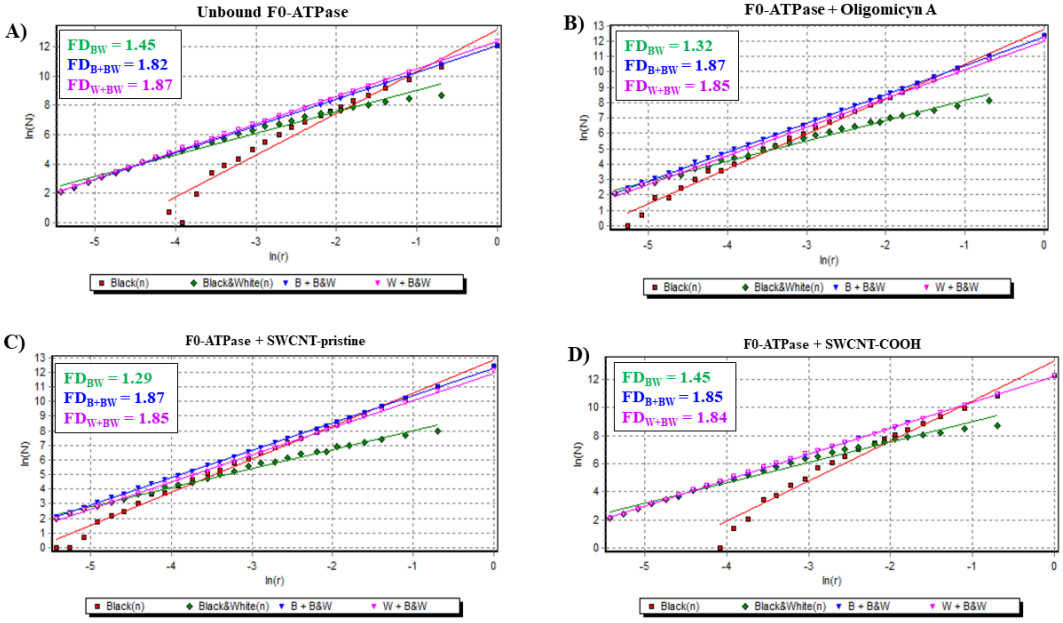

Figure 4. Fractal spectrum based on the box-counting method performed to obtain the slopes of the linear regression yields from binary black/white LPRS maps image-processing. These slopes represent the fractal dimensions (*FD*: D_{BW}, D_{BBW}, and D_{WBW}) for the best docking complexes namely: **A)** unbound F0-ATPase, **B)** oligomycin A/F0-ATPase complex, **C)** SWCNT-pristine/F0-ATPase complex, and **D)** SWCNT-COOH/ F0-ATPase complex.

Herein, the obtained FDs are related to the F0-ATPase surface and backbone non-Euclidean geometry[8, 50] FDs, inform about how the F0-ATPase folding, packing density, solvent-accessibility, and binding-interaction properties could be perturbed under the presence of different ligands forming docking complexes (oligomycin A/F0-ATPase complex, SWCNT-pristine/F0-ATPase complex, and SWCNT-COOH/F0-ATPase complex). In this context, we suggest that, SWCNT-pristine with FD_{BW} = 1.29 lead to a higher change in F0-ATPase roughness-based FD (FD_{BW}) than the SWCNT-COOH (FD_{BW} = 1.45) which exhibits very similar features-based fractal dimension compared physiological condition of unbound F0-ATPase used as control (FD_{BW} = 1.45. These, results fit with the previous on LPRS maps strongly suggesting that the SWCNT-pristine mimicking the nanotoxicological behavior of the specific inhibitor oligomycin A with calculated equal to FD_{BW} = 1.32 also low than the physiological condition of unbound F0-ATPase cited above. As previously cited, a FD ≈ 2 reveals high variety of geometrical information and low self-similarity, while FD ≈ 1 represents little complexity and high self-similarity. By the other hand, the FD-values obtained for

Preprints (www.preprints.org) | NOT PEER-REVIEWED | Posted: 1 September 2020 doi:10.20944/preprints202009.0014.v1

FD_{B+BW} and FD_{W+BW} remain as unperturbed around 1.85 in all the cases revealing high complexity of geometrical information[8, 50].

The results of fractal surface perturbation suggest that the SWCNT-pristine can induce significant changes in the geometrical selectivity of the F0-ATPase like oligomycin A. It is well-known that perturbation (*global* and *local perturbations*) in the three-dimensional spatial arrangement of atoms composing effector residues (*j*-effector allosteric residues) of proteins can be studied using their FDs. Fractal surface-perturbations could negatively impact on catalytic function of F0-ATPase, affecting irreversibly the structural properties of the binding cavities, which are the paramount importance in the complementary processes like substrate recognition and ligand geometrical specificity. [64] Probably, topologically perturbed van der Waals fractal-surface of F0-ATPase after the docking interaction with SWCNT-COOH could theoretically explain the moderate mitochondrial nanotoxicity observed from the SWCNT-COOH/F0-ATPase docking complex (refer to **Figure 3**, **A** and **D**).

Lastly, we carried out a nano-quantitative-structure-toxicity-relationship approaches (Nano-QSRT models) in order to evaluate the influence of additional geometric properties of the ligands SWCNT-pristine and SWCNT-COOH based on the well-known relationship between the topology geometry-based on *n*,*m*-Hamada index with their nanotoxicological properties (*i.e.*, SWCNT-mitotoxicity).

Performed Nano-QSTR models

As reported in the **Material and methods** section, the Nano-QSTR model for SWCNT-pristine was developed using only two variables belonging to the topological index category. The observed vs predicted values and the other relevant statistics, are reported in the **Table 1, Table 2, and Figure 5,** respectively**.**

Table 1. Results of the Nano-QSTR regression model for mitochondrial F0-ATPase inhibition induced by SWCNT-pristine.

SWCNT-pristine (n,m)	Data Observed	Data Predicted	Data Resids	Cross-validation[(a,b)]
amchair 3.3	-20.00000	-18.93350	-1.06650	training
amchair 4.4	-19.70000	-18.83954	-0.86046	training
amchair 5.5	-18.80000	-18.77444	-0.02556	training
amchair 6.6	-18.50000	-18.72592	0.22592	validation
amchair 7.7	-18.20000	-18.68908	0.48908	training
amchair 8.8	-17.50000	-18.66083	1.16083	training
amchair 9.9	-17.20000	-18.63872	1.43872	training
chiral 3.2	-17.20000	-16.28865	-0.91135	validation
chiral 4.1	-17.20000	-15.58908	-1.61092	training
chiral 4.2	-17.00000	-15.84427	-1.15573	training
chiral 4.3	-16.30000	-15.96788	-0.33212	training
chiral 5.1	-16.20000	-15.56891	-0.63109	validation
chiral 5.2	-16.20000	-15.44925	-0.75075	training
chiral 5.3	-16.00000	-15.63349	-0.36651	training
chiral 5.4	-16.00000	-15.72809	-0.27191	training
chiral 6.1	-16.00000	-15.26864	-0.73136	validation
chiral 6.2	-15.90000	-15.19863	-0.70137	training
chiral 6.3	-15.90000	-15.37446	-0.52554	training
chiral 6.4	-15.90000	-15.47126	-0.42874	training
chiral 6.5	-15.80000	-15.39773	-0.40227	validation

Preprints (www.preprints.org) | NOT PEER-REVIEWED | Posted: 1 September 2020 doi:10.20944/preprints202009.0014.v1

chiral 7.1	-15.70000	-15.02346	-0.67654	training
chiral 7.2	-15.40000	-15.17288	-0.22712	training
chiral 7.3	-15.40000	-15.10112	-0.29888	training
chiral 7.4	-15.20000	-15.24345	0.04345	validation
chiral 7.5	-15.20000	-15.34078	0.14078	training
chiral 7.6	-15.20000	-15.28875	0.08875	training
chiral 8.1	-15.00000	-15.03210	0.03210	training
chiral 8.2	-15.00000	-14.77537	-0.22463	validation
chiral 8.3	-14.90000	-15.23422	0.33422	training
chiral 8.4	-14.80000	-15.08583	0.28583	training
chiral 8.5	-14.70000	-15.15833	0.45833	training
chiral 8.6	-14.70000	-15.24567	0.54567	validation
chiral 8.7	-14.70000	-15.20136	0.50136	training
chiral 9.3	-14.60000	-14.79209	0.19209	training
chiral 9.4	-14.50000	-15.12489	0.62489	training
chiral 9.5	-14.50000	-15.11612	0.61612	validation
chiral 9.6	-14.50000	-15.09848	0.59848	training
chiral 9.7	-14.30000	-15.29203	0.99203	training
zig zag 3.0	-14.30000	-15.37860	1.07860	training
zig zag 4.0	-14.10000	-14.00654	-0.09346	validation
zig zag 5.0	-13.70000	-14.00654	0.30654	training
zig zag 6.0	-13.70000	-13.79221	0.09221	training
zig zag 7.0	-13.60000	-13.62087	0.02087	training
zig zag 8.0	-13.30000	-13.48024	0.18024	validation
zig zag 9.0	-12.90000	-13.36294	0.46294	training

Data sets: training [(a)] and validation sets [(b)].

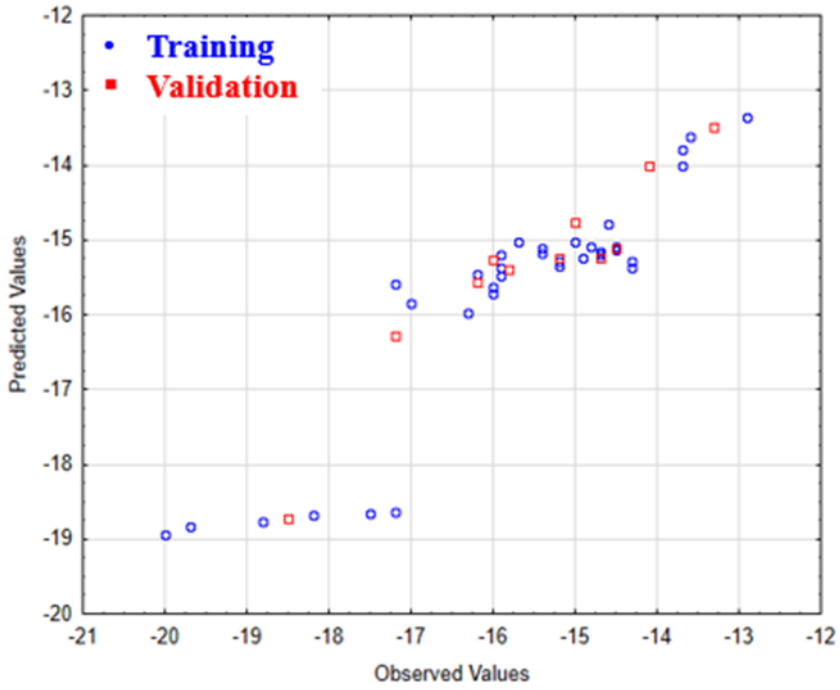

Preprints (www.preprints.org) | NOT PEER-REVIEWED | Posted: 1 September 2020 doi:10.20944/preprints202009.0014.v1

Figure 5. Results of observed vs. predicted values obtained for the Nano-QSTR regression model performed for the SWCNT-pristine data.

Table 2. Results of the relevant statistic parameters obtained from the Nano-QSTR regression model for SWCNT-pristine.

Statistic parameters	Value
Multiple R	0.911445
Multiple R ²	0.830731
Adjusted R ²	0.819811
SS Model	77.70196
df Model	2
MS Model	38.85098
SSResidual	15.83245
df Residual	31
MS Residual	0.510724
F	76.07035
P	0

As can be seen in the **Table 1** and **2**, the Nano-QSTR model shows an overall accuracy and a goodness of fit high, thus indicating this model can be used for a continuous prediction of the likelihood induced mitochondria nanotoxicity inhibition on F0F1-ATPase by interaction with SWCNT-pristine ($f(FEB\_1)$). In this regard, the best Nano-QSTR regression model is based on the linear **equation 11** as:

$$f(FEB\_1) = -8.24425(GNar) + 0.614121(MAXDP) - 2.87142 \quad (\mathbf{11})$$

Afterward, we performed Nano-QSTR model for SWCNT-COOH. For this instance, was carried out a QSTR regression model by using three variables and as in the case of the previous model (i.e., using SWCNT-pristine). Herein, the results obtained on observed vs predicted values, and the other relevant statistics parameters are summarized in the **Table 3, Table 4, and Figure 6,** respectively**.**

Table 3. Results of the Nano-QSTR regression model for mitochondrial F0-ATPase inhibition induced by SWCNT-COOH.

SWCNT-COOH (n,m)	Data Observed	Data Predicted	Data Resids	Cross-validation[a,b]
amchair 3.3	-34.80000	-33.04305	-1.75695	training
amchair 4.4	-33.10000	-31.92664	-1.17336	training
amchair 5.5	-32.30000	-31.36844	-0.93156	training
amchair 6.6	-32.30000	-30.81023	-1.48977	validation
amchair 7.7	-29.80000	-30.53113	0.73113	training
amchair 8.8	-29.10000	-30.25203	1.15203	training
amchair 9.9	-29.00000	-29.97293	0.97293	training
chiral 3.2	-28.50000	-26.92826	-1.57174	validation
chiral 4.1	-27.90000	-26.16358	-1.73642	training

Preprints (www.preprints.org) | NOT PEER-REVIEWED | Posted: 1 September 2020 doi:10.20944/preprints202009.0014.v1

chiral 4.2	-27.60000	-27.01059	-0.58941	training
chiral 4.3	-26.90000	-25.00316	-1.89684	training
chiral 5.1	-26.70000	-28.51704	1.81704	validation
chiral 5.2	-26.60000	-24.71436	-1.88564	training
chiral 5.3	-26.40000	-25.08549	-1.31451	training
chiral 5.4	-26.40000	-24.19447	-2.20553	training
chiral 6.1	-26.30000	-27.20385	0.90385	validation
chiral 6.2	-25.90000	-24.54620	-1.35380	training
chiral 6.3	-25.40000	-25.47553	0.07553	training
chiral 6.4	-25.00000	-24.13724	-0.86276	training
chiral 6.5	-24.80000	-24.44496	-0.35504	validation
chiral 7.1	-24.70000	-25.21534	0.51534	training
chiral 7.2	-24.60000	-26.28422	1.68422	training
chiral 7.3	-24.50000	-24.04522	-0.45478	training
chiral 7.4	-24.30000	-24.52728	0.22728	validation
chiral 7.5	-24.30000	-23.88676	-0.41324	training
chiral 7.6	-24.30000	-23.32855	-0.97145	training
chiral 8.1	-24.10000	-26.95336	2.85336	training
chiral 8.2	-24.10000	-23.51211	-0.58789	validation
chiral 8.3	-24.10000	-25.39320	1.29320	training
chiral 8.4	-24.00000	-24.63822	0.63822	training
chiral 8.5	-23.70000	-24.27680	0.57680	training
chiral 8.6	-23.50000	-22.90990	-0.59010	validation
chiral 8.7	-23.50000	-24.89841	1.39841	training
chiral 9.3	-23.00000	-23.42979	0.42979	training
chiral 9.4	-22.60000	-24.13724	1.53724	training
chiral 9.5	-22.50000	-23.71859	1.21859	validation
chiral 9.6	-22.40000	-23.16039	0.76039	training
chiral 9.7	-22.20000	-23.53151	1.33151	training
zig zag 3.0	-22.10000	-25.42752	3.32752	training
zig zag 4.0	-21.70000	-20.86901	-0.83099	validation
zig zag 5.0	-21.50000	-20.86901	-0.63099	training
zig zag 6.0	-21.40000	-20.17126	-1.22874	training
zig zag 7.0	-21.10000	-19.61305	-1.48695	training
zig zag 8.0	-20.90000	-19.19440	-1.70560	validation
zig zag 9.0	-17.30000	-18.91530	1.61530	training

Data sets: training[(a)] and validation sets[(b)].

Table 4. Results of the relevant statistic parameters obtained from the Nano-QSTR regression model for SWCNT-COOH.

Preprints (www.preprints.org) | NOT PEER-REVIEWED | Posted: 1 September 2020 doi:10.20944/preprints202009.0014.v1

Statistic parameters	Value
Multiple R	0.918915
Multiple R ²	0.844404
Adjusted R ²	0.828845
SS Model	366.1187
df Model	3
MS Model	122.0396
SSResidual	67.46364
df Residual	30
MS Residual	2.248788
F	54.26905
P	0.000000

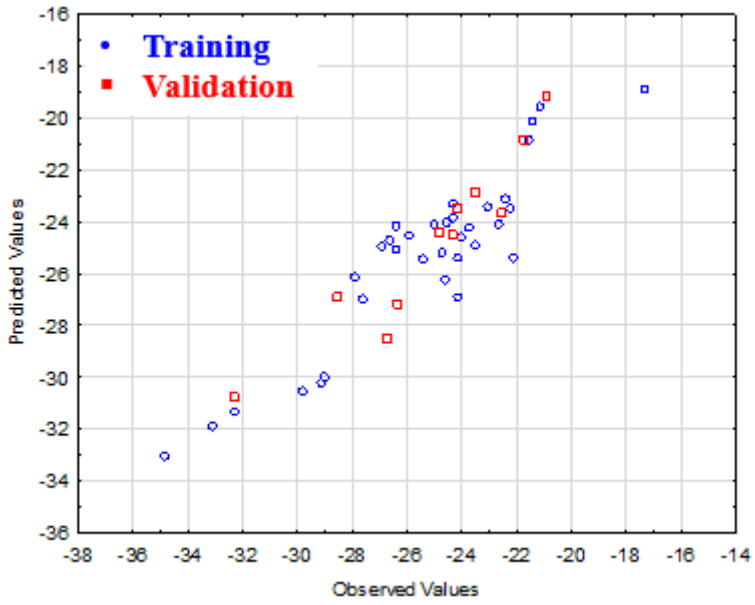

Figure 6. Results of observed vs. predicted values obtained for the Nano-QSTR regression model performed for the SWCNT-COOH data.

For the case of SWCNT-COOH data set the final Nano-QSTR regression model to predicts the mitochondrial F0-ATPase inhibition ($f(FEB\_2)$) is represented by the linear **equation 12** as:

$$f(FEB\_2) = -1005.47(GNar) - 1401.69(PW5) - 139.55(LOC) - 2326.4 \quad (\mathbf{12})$$

Overall, the proposed methodologies rigorously obey the Organization for Economic Co-operation and Development (OECD) and the International Organization for Standardization guidelines for development of alternative methods for Computational Nanotoxicology[51].

Conclusions

In the present study we present a combination of experimental and computational approaches to tackle the SWCNT nanotoxicity based on the mitochondrial F0F1-ATPase inhibition. Experimental evidences supported that the *in vitro* F0F1-ATPase inhibition responses in submitochondrial particles (SMP) are strongly dependent on the higher level of concentration (from 3 to 5 μg/ml) in both types of carbon nanotubes (SWCNT-pristine and SWCNT-COOH) evaluated. In addition, both types of carbon nanotubes show an interaction inhibition pattern for the F0F1-ATPase enzyme, similar to the oligomycin A (specific F0F1-ATPase inhibitor). By the other hand, the best binding pose for the obtained complexes fit well with the previous experimental results. The free energy of binding (FEB-values) for the formed docking complexes following the affinity order as: FEB (oligomycin A/F0-ATPase complex) = -9.8 kcal/mol > FEB (SWCNT-COOH/F0-ATPase complex) = - 6.8 kcal/mol ~ FEB (SWCNT-pristine complex) = -5.9 kcal/mol with relevant interatomic distance of interaction lower than 5 Å, in all the cases and with predominance of van der Waals hydrophobic interactions with critical F0-ATPase binding site residues (Phe 55 and Phe 64) belonging to the same biophysical environment that the oligomycin A inhibitor. In addition, results on elastic network models (LPRS-maps) show that both SWCNT-pristine and SWCNT-COOH promote an abrupt perturbations in several blocks of residues more pronounced for the SWCNT-pristine (strong F0-ATPase nanotoxicity inhibition) than the SWCNT-COOH (moderate F0-ATPase nanotoxicity inhibition) triggering pertubation on the allosteric responses, abnormal signals propagation across inter-residue network of the F0F1-ATPase. In accordance to this, results on fractal-surface of interactions suggest that, the SWCNT-interactions topologically affect the van der Waals fractal-surface of F0-ATPase (SWCNT-pristine > SWCNT-COOH) inducing from strong to moderate mitochondrial nanotoxicity. Lastly, the predictive Nano-QSTR models show that a linear correlation between SWCNT topology and the nanotoxicity induced is present and can be predicted using a Nano-QSTR approach.

Finally, this results open new opportunities toward to the better better understanding of the molecular nanotoxicity mechanisms, relevance of mitotarget-drug discovery and rational drug-design based nanotechnology with potential biomedical application in precision nanomedicine.

Author Contributions: The manuscript was written through the contributions of all authors. All authors have given approval to the final version of the manuscript.

Declaration of interest statement: The authors declare no competing financial interests.

Acknowledgments: The work of M. G.-D., R. C, and M. N. D. S. Cordeiro was supported by UID/QUI/50006/2020 with funding from FCT/MCTES through national funds. J.M.R acknowledges the funding by Xunta de Galicia (ED41E2018/08).

References

1. Fillingame, R. H.; Jiang, W.; Dmitriev, O. Y., Coupling H(+) transport to rotary catalysis in F-type ATP synthases: structure and organization of the transmembrane rotary motor. **2000,** *203* (1), 9-17.
2. Mitchell, P., Coupling of Phosphorylation to Electron and Hydrogen Transfer by a Chemi-Osmotic type of Mechanism. *Nature* **1961,** *191* (4784), 144-148.
3. Bulygin, V. V.; Duncan, T. M.; Cross, R. L., Rotor/Stator interactions of the epsilon subunit in Escherichia coli ATP synthase and implications for enzyme regulation. *The Journal of biological chemistry* **2004,** *279* (34), 35616-21.
4. Abrahams, J. P.; Buchanan, S. K.; Van Raaij, M. J.; Fearnley, I. M.; Leslie, A. G.; Walker, J. E., The structure of bovine F1-ATPase complexed with the peptide antibiotic efrapeptin. *Proc Natl Acad Sci U S A* **1996,** *93* (18), 9420-9424.
5. Senior, A. E., The structure of mitochondrial ATPase. *Biochimica et Biophysica Acta (BBA) - Reviews on Bioenergetics* **1973,** *301* (3), 249-277.
6. Yang, Z.; Zhang, Y.; Yang, Y.; Sun, L.; Han, D.; Li, H.; Wang, C., Pharmacological and toxicological target organelles and safe use of single-walled carbon nanotubes as drug carriers in treating Alzheimer disease. *Nanomedicine : nanotechnology, biology, and medicine* **2010,** *6* (3), 427-41.
7. González-Durruthy, M.; Giri, A. K.; Moreira, I.; Concu, R.; Melo, A.; Ruso, J. M.; Cordeiro, M. N. D. S., Computational modeling on mitochondrial channel nanotoxicity. *Nano Today* **2020,** *34*, 100913.

8. González-Durruthy, M.; Manske Nunes, S.; Ventura-Lima, J.; Gelesky, M. A.; González-Díaz, H.; Monserrat, J. M.; Concu, R.; Cordeiro, M. N. D. S., MitoTarget Modeling Using ANN-Classification Models Based on Fractal SEM Nano-Descriptors: Carbon Nanotubes as Mitochondrial F0F1-ATPase Inhibitors. *Journal of Chemical Information and Modeling* **2019,** *59* (1), 86-97.
9. Atwal, K. S.; Ahmad, S.; Ding, C. Z.; Stein, P. D.; Lloyd, J.; Hamann, L. G.; Green, D. W.; Ferrara, F. N.; Wang, P.; Rogers, W. L.; Doweyko, L. M.; Miller, A. V.; Bisaha, S. N.; Schmidt, J. B.; Li, L.; Yost, K. J.; Lan, H.-J.; Madsen, C. S., N-[1-Aryl-2-(1-imidazolo)ethyl]-guanidine derivatives as potent inhibitors of the bovine mitochondrial F1F0 ATP hydrolase. *Bioorganic & Medicinal Chemistry Letters* **2004,** *14* (4), 1027-1030.
10. Atwal, K. S.; Wang, P.; Rogers, W. L.; Sleph, P.; Monshizadegan, H.; Ferrara, F. N.; Traeger, S.; Green, D. W.; Grover, G. J., Small molecule mitochondrial F1F0 ATPase hydrolase inhibitors as cardioprotective agents. Identification of 4-(N-arylimidazole)-substituted benzopyran derivatives as selective hydrolase inhibitors. *Journal of medicinal chemistry* **2004,** *47* (5), 1081-4.
11. Liu, J.; Yuan, B.; Wu, X.; Li, J.; Han, F.; Dou, Y.; Chen, M.; Yang, Z.; Yang, K.; Ma, Y., Modulated enhancement in ion transport through carbon nanotubes by lipid decoration. *Carbon* **2017,** *111*, 459-466.
12. González-Durruthy, M.; Castro, M.; Nunes, S. M.; Ventura-Lima, J.; Alberici, L. C.; Naal, Z.; Atique-Sawazaki, D. T.; Curti, C.; Ruas, C. P.; Gelesky, M. A.; Roy, K.; González-Díaz, H.; Monserrat, J. M., QSPR/QSAR-based Perturbation Theory approach and mechanistic electrochemical assays on carbon nanotubes with optimal properties against mitochondrial Fenton reaction experimentally induced by Fe2+-overload. *Carbon* **2017,** *115*, 312-330.
13. González-Durruthy, M.; Werhli, A. V.; Seus, V.; Machado, K. S.; Pazos, A.; Munteanu, C. R.; González-Díaz, H.; Monserrat, J. M., Decrypting Strong and Weak Single-Walled Carbon Nanotubes Interactions with Mitochondrial Voltage-Dependent Anion Channels Using Molecular Docking and Perturbation Theory. *Scientific Reports* **2017,** *7* (1), 13271.
14. González-Durruthy, M.; Werhli, A. V.; Cornetet, L.; Machado, K. S.; González-Díaz, H.; Wasiliesky, W.; Ruas, C. P.; Gelesky, M. A.; Monserrat, J. M., Predicting the binding properties of single walled carbon nanotubes (SWCNT) with an ADP/ATP mitochondrial carrier using molecular docking, chemoinformatics, and nano-QSBR perturbation theory. *RSC Advances* **2016,** *6* (63), 58680-58693.
15. Halestrap, A. P., The C Ring of the F1Fo ATP Synthase Forms the Mitochondrial Permeability Transition Pore: A Critical Appraisal. *Frontiers in oncology* **2014,** *4*, 234.
16. Alavian, K. N.; Beutner, G.; Lazrove, E.; Sacchetti, S.; Park, H.-A.; Licznerski, P.; Li, H.; Nabili, P.; Hockensmith, K.; Graham, M.; Porter, G. A.; Jonas, E. A., An uncoupling channel within the c-subunit ring of the F₁F_O ATP synthase is the mitochondrial permeability transition pore. **2014,** *111* (29), 10580-10585.
17. Shchepina, L. A.; Pletjushkina, O. Y.; Avetisyan, A. V.; Bakeeva, L. E.; Fetisova, E. K.; Izyumov, D. S.; Saprunova, V. B.; Vyssokikh, M. Y.; Chernyak, B. V.; Skulachev, V. P., Oligomycin, inhibitor of the F0 part of H+-ATP-synthase, suppresses the TNF-induced apoptosis. *Oncogene* **2002,** *21* (53), 8149-57.
18. Szklarczyk, R.; Nooteboom, M.; Osiewacz, H. D., Control of mitochondrial integrity in ageing and disease. *Philos Trans R Soc Lond B Biol Sci* **2014,** *369* (1646), 20130439-20130439.
19. Ponnalagu, D.; Singh, H., Insights Into the Role of Mitochondrial Ion Channels in Inflammatory Response. *Frontiers in physiology* **2020,** *11*, 258.
20. Missiroli, S.; Patergnani, S.; Caroccia, N.; Pedriali, G.; Perrone, M.; Previati, M.; Wieckowski, M. R.; Giorgi, C., Mitochondria-associated membranes (MAMs) and inflammation. *Cell death & disease* **2018,** *9* (3), 329.
21. Trott, O.; Olson, A. J., AutoDock Vina: improving the speed and accuracy of docking with a new scoring function, efficient optimization, and multithreading. *J Comput Chem* **2010,** *31* (2), 455-461.
22. Forli, S.; Huey, R.; Pique, M. E.; Sanner, M. F.; Goodsell, D. S.; Olson, A. J., Computational protein-ligand docking and virtual drug screening with the AutoDock suite. *Nature protocols* **2016,** *11* (5), 905-19.
23. Lavecchia, A., Machine-learning approaches in drug discovery: methods and applications. *Drug Discovery Today* **2015,** *20* (3), 318-331.
24. Chennubhotla, C.; Bahar, I., Signal Propagation in Proteins and Relation to Equilibrium Fluctuations. *PLOS Computational Biology* **2007,** *3* (9), e172.
25. Concu, R.; Dea-Ayuela, M. A.; Perez-Montoto, L. G.; Bolas-Fernández, F.; Prado-Prado, F. J.; Podda, G.; Uriarte, E.; Ubeira, F. M.; González-Díaz, H., Prediction of Enzyme Classes from 3D Structure: A General Model and Examples of Experimental-Theoretic Scoring of Peptide Mass Fingerprints of Leishmania Proteins. *Journal of Proteome Research* **2009,** *8* (9), 4372-4382.
26. Ghasemi, J.; Saaidpour, S., QSPR prediction of aqueous solubility of drug-like organic compounds. *Chemical & pharmaceutical bulletin* **2007,** *55* (4), 669-74.
27. Del Rio, A.; Piras, P., Enantiophore modeling in 3D-QSAR. A data mining application on Whelk-O1 chiral stationary phase. *Chirality* **2006,** *18*, 498-508.
28. Zhang, S.; Golbraikh, A.; Tropsha, A., Development of Quantitative Structure−Binding Affinity

Relationship Models Based on Novel Geometrical Chemical Descriptors of the Protein−Ligand Interfaces. *Journal of medicinal chemistry* **2006,** *49*, 2713-24.
29. Burello, E.; Worth, A. P., QSAR modeling of nanomaterials. *Wiley interdisciplinary reviews. Nanomedicine and nanobiotechnology* **2011,** *3* (3), 298-306.
30. Fourches, D.; Pu, D.; Tassa, C.; Weissleder, R.; Shaw, S. Y.; Mumper, R. J.; Tropsha, A., Quantitative Nanostructure−Activity Relationship Modeling. *ACS Nano* **2010,** *4* (10), 5703-5712.
31. Buglak, A. A.; Zherdev, A. V.; Dzantiev, B. B., Nano-(Q)SAR for Cytotoxicity Prediction of Engineered Nanomaterials. *Molecules* **2019,** *24* (24), 4537.
32. Basant, N.; Gupta, S., Multi-target QSTR modeling for simultaneous prediction of multiple toxicity endpoints of nano-metal oxides. *Nanotoxicology* **2017,** *11* (3), 339-350.
33. Concu, R.; Kleandrova, V. V.; Speck-Planche, A.; Cordeiro, M., Probing the toxicity of nanoparticles: a unified in silico machine learning model based on perturbation theory. *Nanotoxicology* **2017,** *11* (7), 891-906.
34. Ahmadi, S., Mathematical modeling of cytotoxicity of metal oxide nanoparticles using the index of ideality correlation criteria. *Chemosphere* **2020,** *242*, 125192.
35. Mu, Y.; Wu, F.; Zhao, Q.; Ji, R.; Qie, Y.; Zhou, Y.; Hu, Y.; Pang, C.; Hristozov, D.; Giesy, J. P.; Xing, B., Predicting toxic potencies of metal oxide nanoparticles by means of nano-QSARs. *Nanotoxicology* **2016,** *10* (9), 1207-14.
36. Toropova, A. P.; Toropov, A. A.; Veselinovic, A. M.; Veselinovic, J. B.; Benfenati, E.; Leszczynska, D.; Leszczynski, J., Nano-QSAR: Model of mutagenicity of fullerene as a mathematical function of different conditions. *Ecotoxicol Environ Saf* **2016,** *124*, 32-36.
37. Toropov, A. A.; Toropova, A. P., Quasi-SMILES and nano-QFAR: united model for mutagenicity of fullerene and MWCNT under different conditions. *Chemosphere* **2015,** *139*, 18-22.
38. Toropova, A. P.; Toropov, A. A., Mutagenicity: QSAR - quasi-QSAR - nano-QSAR. *Mini Rev Med Chem* **2015,** *15* (8), 608-21.
39. Toropova, A. P.; Toropov, A. A.; Benfenati, E.; Korenstein, R.; Leszczynska, D.; Leszczynski, J., Optimal nano-descriptors as translators of eclectic data into prediction of the cell membrane damage by means of nano metal-oxides. *Environ Sci Pollut Res Int* **2015,** *22* (1), 745-57.
40. Liu, R.; Rallo, R.; Weissleder, R.; Tassa, C.; Shaw, S.; Cohen, Y., Nano-SAR development for bioactivity of nanoparticles with considerations of decision boundaries. *Small* **2013,** *9* (9-10), 1842-52.
41. Tantra, R.; Oksel, C.; Puzyn, T.; Wang, J.; Robinson, K. N.; Wang, X. Z.; Ma, C. Y.; Wilkins, T., Nano(Q)SAR: Challenges, pitfalls and perspectives. *Nanotoxicology* **2015,** *9* (5), 636-42.
42. Argese, E.; Bettiol, C.; Giurin, G.; Miana, P., Quantitative structure—activity relationships for the toxicity of chlorophenols to mammalian submitochondrial particles. *Chemosphere* **1999,** *38* (10), 2281-2292.
43. Ferguson, S. J.; Sorgato, M. C., The phosphorylation potential generated by respiring bovine heart submitochondrial particles. *Biochem J* **1977,** *168* (2), 299-303.
44. Argese, E.; Bettiol, C.; Ghelli, A.; Todeschini, R.; Miana, P., Submitochondrial particles as toxicity biosensors of chlorophenols. **1995,** *14* (3), 363-368.
45. Sorgato, M. C.; Branca, D.; Ferguson, S. J., The rate of ATP synthesis by submitochondrial particles can be independent of the magnitude of the protonmotive force. *Biochem J* **1980,** *188* (3), 945-948.
46. Berman, H. M.; Westbrook, J.; Feng, Z.; Gilliland, G.; Bhat, T. N.; Weissig, H.; Shindyalov, I. N.; Bourne, P. E., The Protein Data Bank. *Nucleic Acids Research* **2000,** *28* (1), 235-242.
47. Feinstein, W. P.; Brylinski, M., Calculating an optimal box size for ligand docking and virtual screening against experimental and predicted binding pockets. *J Cheminform* **2015,** *7*, 18.
48. Oliwa, T.; Shen, Y., cNMA: a framework of encounter complex-based normal mode analysis to model conformational changes in protein interactions. *Bioinformatics* **2015,** *31* (12), i151-i160.
49. srl, K. *Dragon (software for molecular descriptor calculation)*, 7.0.10; Italy, 2017.
50. González-Durruthy, M.; Scanavachi, G.; Rial, R.; Liu, Z.; Cordeiro, M. N. D. S.; Itri, R.; Ruso, J. M., Mapping the underlying mechanisms of fibrinogen benzothiazole drug interactions using computational and experimental approaches. *International Journal of Biological Macromolecules* **2020,** *163*, 730-744.
51. OECD Principles for the Validation, for Regulatory Porposes of (Quantitative) Structure Activity Relationship Model. (accessed on13/03/2020).